HHS Public Access

Author manuscript

Biomaterials. Author manuscript; available in PMC 2021 November 22.

Published in final edited form as:

Biomaterials. 2021 September ; 276: 120989. doi:10.1016/j.biomaterials.2021.120989.

Osmotic core-shell polymeric implant for sustained BDNF AntagoNAT delivery in CNS using minimally invasive nasal depot (MIND) approach

Smrithi Padmakumar[a], **Gregory Jones**[a], **Olga Khorkova**[b], **Jane Hsiao**[b], **Jonghan Kim**[c], **Benjamin S. Bleier**[d], **Mansoor M. Amiji**[a,*]

[a]'Department of Pharmaceutical Sciences, School of Pharmacy, Northeastern University, Boston, MA, USA

[b]Opko Health, Miami, FL, USA

[c]Department of Biomedical and Nutritional Sciences, Zuckerberg College of Health Sciences, University of Massachusetts at Lowell, Lowell, MA, USA

[d]Massachusetts Eye and Ear Infirmary, Harvard Medical School, Boston, MA, USA

Abstract

The development of drug delivery strategies for efficacious therapeutic administration directly into the central nervous system (CNS) in a minimally invasive manner remains a major obstacle hindering the clinical translation of biological disease-modifying therapeutics. A novel direct *trans*-nasal delivery method, termed 'Minimally-Invasive Nasal Depot' (MIND), has proved to be successful in providing high CNS uptake and brain distribution of blood-brain barrier (BBB) impermeant therapeutics via direct administration to the olfactory submucosal space in a rodent model. The present study describes the engineering of custom-made implants with a unique architecture of an "osmotically-active core" entrapping the therapeutic and a "biodegradable polymeric shell" to enable long-acting delivery using the MIND procedure. The MIND-administered implant provided sustained CNS delivery of brain derived neurotrophic factor (BDNF) AntagoNATs for up to 4 weeks in Sprague Dawley rats resulting in significant endogenous BDNF protein upregulation in several brain tissues. The biocompatibility of such core-shell implants coupled with their substantial pharmacokinetic advantages and safety of the MIND procedure highlights the practical utility and translational potential of this synergistic approach for treatment of chronic age-related neurodegenerative diseases.

*Corresponding author. m.amiji@northeastern.edu (M.M. Amiji).

Declaration of competing interest

The authors declare that they have no known competing financial interests or personal relationships that could have appeared to influence the work reported in this paper.

Appendix A. Supplementary data

Supplementary data to this article can be found online at https://doi.org/10.1016/j.biomaterials.2021.120989.

Keywords

Osmotic implant; Brain-derived neurotrophic factor; AntagoNAT; Minimially-invasive nasal depot (MIND); Neurodegenerative diseases; CNS Delivery

1. Introduction

Neurodegeneration refers to the progressive atrophy or irreversible damage to the structure and/or function of specific subsets of neurons of brain and spinal cord which ultimately results in their death [1–3]. This leads to a large group of debilitating disorders manifesting heterogenous pathological characteristics that affect approximately 30 million people worldwide while the treatment options still remain scarce [4,4–6]. Aging is the primary risk factor for the escalating burden of such disorders, such as Alzheimer's disease (AD) or Parkinson's disease (PD) [6, 7]. Apart from being ineffective, the currently available drugs used for alleviating disease symptoms exert toxic side effects [5,6].

Brain derived neurotrophic factor (BDNF) is a neurotrophin important for the survival, differentiation and maturation of neurons of the nervous system [8,9]. BDNF protein and mRNA levels have been detected in the majority of adult brain sub-regions such as olfactory bulb, cortex, hippocampus, basal forebrain, hypothalamus, mesencephalon and brainstem [10,11]. Reduced expression of BDNF in the nigrostriatal dopaminergic brain regions has been implicated in the pathogenesis of Parkinson's disease [12–15]. Additionally, insufficient supply of neuronal BDNF leads to defects in synaptic plasticity, thereby leading to neurodegeneration [13]. Therefore, there is a clear need for the development of therapeutic interventions aimed at increasing BDNF levels for neuroprotective as well as neurorestorative treatment arms [16,17]. On the other hand, there are several challenges that hinder the development and engineering of recombinant BDNF protein therapies: a complex synthetic process, the existence of multiple active BDNF isoforms binding to different receptors, the highly intricate structure of the BDNF gene, and the regulation of its expression at multiple levels [18–22]. Compounding these issues are the physico-chemical properties of neurotrophins that do not allow them to cross the blood-brain barrier (BBB) and further complicate central nervous system (CNS) delivery [23].

Oligonucleotides are gaining attention specifically as candidates for neurodegenerative disease therapy owing to high target specificity and accessibility, wide CNS distribution, and negligible toxicity concerns [23,24]. In contrast to some recombinant proteins, oligonucleotides have a more straightforward path to clinical translation and large scale commercial development, partly due to more defined constituent chemistry and precise synthetic processes. BDNF AntagoNATs are single stranded short synthetic oligonucleotide-based compounds possessing the ability to inhibit BDNF-AS, the conserved noncoding natural antisense transcript (NAT) which normally slows down BDNF sense RNA transcription and represses endogenous BDNF protein production. It has been previously reported that BDNF AntagoNAT (BDNF AT) treatment can induce BDNF mRNA and protein upregulation and *in vitro* differentiation and *in vivo* proliferation of neuronal cells [17]. Nevertheless, the BBB-impermeant nature of such ATs typically requires invasive

modes of CNS delivery such as intrathecal (IT) or intracerebroventricular (ICV) routes wherein the BBB is physically breached [23]. Such routes are associated with significant potential adverse effects such as brain edema, hemorrhage, seizures, cerebrospinal fluid (CSF) leak, catheter related complications, infections, and in rare cases death [25,26].

Intranasal administration, one potential alternative to direct CNS administration, has been reported to bypass the BBB in a non-invasive manner and deliver therapeutics including both small and macromolecules to the brain within a short period of time [27]. However, it has not been successfully clinically adopted owing to the pitfalls associated with uniformity of delivered dose, poor drug distribution, limited mucosal retention, and restricted *trans*-epithelial diffusion [28]. In this context, our group exploited the direct *trans*-nasal, *trans*-olfactory pathway to CNS through the direct submucosal implantation of a therapeutic depot. This 'Minimally Invasive Nasal Depot (MIND)' [28] technique is based on the routine endoscopic guided intranasal procedures performed by otorhinolaryngologists and provides a direct route of access to the basolateral aspect of the olfactory epithelium (OE) thereby enabling direct CNS delivery. Our previously reported rat model of MIND could recapitulate the anatomy of the proposed clinical depot delivery technique [28]. The procedure was found to be well tolerated by animals while eliminating the need for invasive BBB penetrating techniques such as ICV administration [28]. The administration of BDNF AT formulations (AT dispersed in thermosensitive Pluronic F-127 gel and AT liposomes-in gel suspension) to the submucosal compartment of rat OE by the MIND technique provided efficient and consistent dose delivery within the tissue surrounding the olfactory neurons [28]. MIND administration also provided high CNS uptake of the otherwise impermeant BDNF AT with a relative delivery efficiency approaching 40% of the direct ICV route. We further demonstrated that a single dose significantly increased BDNF proteins levels in different subregions of brain up to 4 days post administration [28] confirming the therapeutic translational potential of this method.

The purpose of this study was to build on our prior data and develop implantable formulation from biodegradable polymers to further extend the release profile of therapeutics such as BDNF AT. We exploited the concept of custom-made core-shell implants with a unique design of an "osmotically-active core" and a "biodegradable shell" with tailorable dimensions, shapes and properties specifically amenable for MIND implantation. Unlike other biodegradable polymer implants, an osmotic core-shell implant design is highly versatile from an engineering perspective, can accommodate a variety of payloads and can be custom-designed for different therapeutic indications. We subsequently investigated the pharmacokinetic and pharmacodynamic advantages of sustained BDNF AT delivery and the *in vivo* safety profile of the 'MIND Implant' approach in healthy animals.

2. Experimental methods

2.1. Materials

Poly (epsilon-caprolactone) (PCL, molecular weight of 50 kDa) and the organic solvent 2,2,2-trifluoroethanol (2,2,2-TFE) were purchased from Polysciences Inc. (Warrington, PA) and Acros Organics (Fair Lawn, NJ) respectively. Pluronic F-127 was obtained from BASF Corp. (Florham Park, NJ). BDNF expressing AntagoNAT was provided by Opko Health

(Miami, FL). The dye, fluorescein isothiocyanate (FITC) -Dextran (average molecular weight 3–5 kDa) used for *in vitro* release studies and EDTA-free Protease Inhibitor tablet used for making the tissue homogenization buffer were procured from Sigma Aldrich (St. Louis, MO). Pierce BCA assay kit for protein quantification, ELISA Femto Solution Mix and 96 well white NuncTM plates used for the BDNF AT hybridization assay were obtained from Thermo Fisher Scientific (Waltham, MA). The capture and detection probes used for hybridization assay were designed by Qiagen Inc. (Germantown, MD). 4x SSC/0.5% sarkosyl, 10% (v/v) neutral buffered formalin and histoplast paraffin wax were bought from Fisher Scientific (Fair Lawn, NJ). Streptavidin-HRP conjugate used for the hybridization assay was procured from Jackson Immuno-Research (West Grove, PA). ChemiKine Brain Derived Neurotrophic Factor sandwich ELISA kit for BDNF level quantification was purchased from Millipore Sigma (Burlington, MA). The drill used in *in vivo* surgery protocol was obtained from Dremel (Mt. Prospect, IL) and 5–0 nylon sutures used for incision closure were purchased from Med-Vet International (Mettawa, IL).

2.2. Methods

2.2.1. Fabrication of BDNF AT-loaded osmotic core-shell implants—BDNF AT loaded osmotic core-shell implants were fabricated in a step-wise manner as described below.

2.2.1.1. Fabrication of biodegradable PCL shell.: The biodegradable polycaprolactone (PCL) shell was fabricated using the conventional technique of dip-coating. For this, PCL solutions of different concentrations in the range of 10–14 w/v% were pre-formed by dissolving the polymer in the organic solvent 2,2,2-trifluoroethanol (TFE). A lubricated cylindrical glass rod of ~5 mm diameter (coating substrate) was then dipped into the PCL-TFE solution of optimized concentration for ~1 min. The dipped rod was then pulled out of the solution and air-dried. The number of dipping-drying cycles was optimized so as to obtain a thick polymeric sheath. The fabricated PCL shells were subjected to overnight vacuum drying in a desiccator at room temperature to facilitate the complete removal of residual organic solvent. PCL shells were thereafter carefully peeled off from the substrate rods thereby forming hollow reservoirs. The shell wall thickness was measured using a micrometer screw gauge (Eisco, Victor, NY).

2.2.1.2. Fabrication of BDNF AT-loaded osmotic core.: The osmotic core component of the implant is constituted of thermosensitive Pluronic F-127 gel. A 30 w/v% solution was pre-formed by dissolving Pluronic F-127 in 1X PBS at 4 °C upon continuous stirring. BDNF AT pre-aliquoted in water (2 mg/mL concentration) was added to 300 μL of homogenous Pluronic F-127 solution under stirring. The thermogelling property of Pluronic F-127 was exploited to formulate a gel-based osmotic core at room temperature.

2.2.1.3. Assembly of final core-shell implant.: The volume of Pluronic F-127 gel entrapping BDNF AT corresponding to the *in vivo* therapeutic BDNF AT dose for rats (0.15 mg/kg) or the gel alone without BDNF AT was added into the fabricated biodegradable PCL shell reservoir, keeping the shell in a vertical position. After this step, the remnant length of shell was shortened and its open end was sealed with heat using a cautery pen.

2.2.2. Characterization of PCL shell morphology—The morphology of PCL shell surface was qualitatively assessed by field emission scanning electron microscopy (FESEM) (Hitachi S-4800 FESEM, Tokyo, Japan). The samples were sputter coated with 5 nm of platinum using a sputter-coater (Cressington 208HR, Watford, UK) and imaged with an accelerating voltage of 3 kV.

2.2.3. In vitro release of FITC dextran from core-shell implant—Implants were fabricated according to the above-mentioned procedure with fluorescein isothiocyanate (FITC)-Dextran dye (2 mg/mL) as the payload. They were then immersed in Phosphate Buffered Saline (PBS) reservoir (pH 7.4, 37 °C, 100 rpm shaking). At time points such as 0, 3, 6, 24, 48 h, 6, 11, 21 and 29 days, a definite volume was retrieved from the PBS reservoir and thereafter replenished with the same volume of fresh PBS to facilitate sink conditions. FITC fluorescence intensity of the collected aliquots were measured using a plate reader (Biotek, Winooski, VT) at excitation and emission wavelengths of 490 and 520 nm respectively. Cumulative FITC-dextran release was calculated and plotted as a function of time.

2.2.4. In vivo administration of the implants using MIND approach in Sprague Dawley rats—The guidelines developed by the Institutional Animal Care and Use Committee (IACUC) of Northeastern University were followed for designing our animal experiments. Sprague Dawley rats (males, 250–300 g weight) were procured from Charles River Laboratories (Wilmington, MA) for the study. All animals were provided with drinking water and diet *ad libitum* and they were maintained under standard conditions of 12 h light cycle/12 h dark cycle.

The *in vivo* surgical implantation of core-shell implants in naïve rats was carried out with the MIND protocol developed by our team previously [28]. Rats anesthetized with 2% isoflurane were placed on a stereotactic apparatus equipped with ear bars and body temperatures were maintained at 37 °C. The surgical site at located at the snout was prepped aseptically with povidone iodine and alcohol. A 1 cm long midline sagittal incision was made with a sterile scalpel blade followed by the elevation of bilateral skin flaps to expose the underlying paired nasal bones. Thes nasal bones were removed using a high speed surgical drill without disturbing the deep layer of basolateral olfactory mucoperiosteum. This exposure provided for a subcutaneous cavity in direct contact with the basolateral olfactory epithelium. The implant, composed of BDNF AT entrapped in gel osmotic core and PCL shell (pre-sterlized by UV irradiation), was inserted into this cavity followed by closure of the skin incision using 5–0 nylon suture. Animals were randomly assigned to five groups and sacrificed at day 4, 7, 14, 21 or 28 (n = 4 rats/group) post-surgery. Control groups consisted of both age and sex matched untreated naïve animals as well as animals treated with placebo implants containing the Pluronic F-127 gel core without any BDNF AT payload. All animals subjected to the MIND procedure were monitored daily for any signs of health deterioration or changes in normal behavior throughout the study period of 28 days.

2.2.5. In vivo distribution of BDNF at levels in rat brain sub-regions—Rats implanted with BDNF AT core-shell implants via MIND approach were sacrificed at

the above-mentioned time points post-surgery. Blood samples were collected by cardiac puncture prior to euthanasia so as to quantify the BDNF AT levels in plasma collected as supernatants upon centrifugation for 10 min at 2000 g and 4 °C. Following the sacrifice procedure, rat brains were harvested and various sub-regions of interest were isolated based on rat brain atlas coordinates along with the olfactory bulb (OB). Samples from striatum (STR), hippocampus (HC), substantia nigra (SN) and cerebellum (CB) were retrieved using 3 mm tissue biopsy punches, which were thereafter homogenized with ice-cold tissue lysis buffer constituted by dissolving 10 mM Tris-HCl at pH 7, 0.4 mM EDTA, 100 mM NaCl, 2 g BSA, 1.54 mM sodium azide and 2% Triton X-100 in 100 mL of water added with EDTA-free Protease Inhibitor tablet. Total protein samples from tissue homogenates were collected as supernatants after a 20 min centrifugation at 20,000*g* and protein content was quantified with standard BCA assay. The BDNF AT levels in these tissue extracts as well as plasma samples were quantified by AT hybridization assay described previously [28].

For the BDNF AT sequence: 5′-C*A*T*A*G*G*A*-
G*A*C*C*C*T*C*C*G*C*A*A*C-3′

Capture probe and detection probes were designed with sequences given below, such that they were complementary to the 3′ and 5’ ends of BDNF AT respectively.

Capture probe sequence - (5AmMC12//iSp18/iSp18//
G*+T*+T*+G*+C*+G*+G*+A*+G).

Detection probe sequence -(+G*+G*+T*+C*+T*+C*+C*+T*+A*+T*+G/iSp18//iSp18//
iBiodT//3BioTEG).

Wherein * refers to phosphorothioate bond, + to LNA modifications, iSp18 to internal 18-mer spacer, 5AMmc12 to 5′-amino modifier C12 m, 3BioTEG to 3′ biotin-TEG and iBiodT to internal biotin-dT.

A 96-well white NuncTM plate was coated with a solution made by dissolving 40 μL of 5000 pmol/mL capture probe to 19.96 mL of capture probe buffer. BSA blocking was done as the next step followed by thermal annealing of samples added with detection probe. The detection probe solution was made by adding 200 μL of 5000 pmol/mL detection probe in 19.8 mL of buffer constituted by 4X SSC/0.5% sarkosyl. A streptavidin-HRP conjugate diluted at 1: 50,000 ratio was subsequently added to the washed plate. An incubation step at 37 °C for 30 min was then followed by washes. Finally, the wells were added with 150 μL of the ELISA Femto Solution Mix and luminescence read outs were taken immediately with a plate reader (Biotek, Winooski, VT). The calculated BDNF AT levels were normalized to the amount of protein in each sample and expressed as pg AT/μg protein.

2.2.6. Pharmacokinetic analysis of BDNF at concentration in rat brain sub-regions—AntagoNAT amounts per gram tissue were converted to concentration (i.e., pg/mL) using reported values for rat brain density [29] in order to facilitate future modeling and simulation. Noncompartmental analysis (NCA) of the concentration-time data was performed using the SimBiology application within the MATLAB software (version#2020a) [30]. The maximum concentration (C_{max}) and time of maximum concentration (t_{max})

were determined using SimBiology and verified graphically. The area under the tissue concentration-time curve (AUC) from time zero to the last measured time (AUC0-last) was determined using the linear trapezoidal method. The area under the first moment concentration-time curve was calculated from time zero to the last measured time (AUMC0-last) using the linear trapezoidal method. Due to the lack of reliable terminal data points, namely in deep brain tissues, terminal slope analysis was not performed, and consequently AUC or AUMC analysis was not extended to time infinity. Mean residence time (MRT) was calculated as the ratio of AUMC and AUC (i.e., MRT = AUMC/AUC).

2.2.7. Quantification of BDNF protein levels in brain sub-regions—BDNF protein de-repression levels in each extracted protein sample were analyzed using BDNF sandwich ELISA kits according to the manufacturer's protocol. The calculated BDNF protein concentration values were normalized to the amount of total protein in each sample and expressed as pg of BDNF per μg of protein.

2.2.8. Pharmacokinetic analysis of in vivo BDNF response—The tissue levels of BDNF in treated animals were baseline corrected using BDNF levels from naïve animals. NCA of the concentration-time curve of BDNF protein was performed using SimBiology/MATLAB. The maximal concentration (C_{max}) and time of maximal concentration (t_{max}) were determined with SimBiology and verified graphically. The area under the effect curve was determined via the linear trapezoidal method, and the analysis was restricted from time zero to the last measured time ($AUEC_{0\text{-}last}$) due to inconsistent terminal data.

2.2.9. Comparisons of delivery efficiencies between core-shell implant and depot injection—The performance of the implant formulation was evaluated in comparison to the previously reported AT-Gel depot formulation [28]. As previously reported, kinetic parameters for the depot were determined from 0 to 96 h and not extended to time infinity due to unreliable terminal data points. Subsequently, the kinetic parameters such as C_{max} and AUC of MIND core-shell implants were compared relative to those for depot and the percent changes were determined.

2.2.10. Analysis of explanted osmotic implants for residual BDNF AT—Upon euthanasia, the implants were carefully inspected for any visual changes in shape, morphology and integrity following which they were explanted from the olfactory submucosal space of animals. The weights were recorded and compared to the weight of the exact implant measured prior to MIND administration. The implants were then cut open to retrieve the remaining gel which was subjected to nanodrop quantification of BDNF AT. These values subtracted from the initially loaded BDNF AT amount gave the amount of AT released from the implant at that time-point. The cumulative AT release was then calculated to plot the *in vivo* AT release profile over time. The surface features of explanted implants were qualitatively assessed by FESEM in order to study the morphological alterations over time.

2.2.11. Histological analysis of explanted osmotic implants—The surgical sites of all animals subjected to MIND implantation were closely monitored throughout the study frame for any signs of infection, edema or inflammation. After sacrifice, the rat

nasal cavities were opened and visually inspected for any signs of infection around the implant. Nasal tissues at the implant-nasal cavity interface were collected from the snouts of animals subjected to MIND implantation upon sacrifice at different time points. The tissue samples were fixed in 10% (v/v) neutral buffered formalin, embedded in paraffin wax and sectioned by microtome at a thickness of 5 μm for standard histology analysis. Staining was done with hematoxylin and eosin (H&E) and slides were imaged with a camera-equipped microscope (Keyence BZX710 All-in-One Fluorescence Microscope, Itasca, IL) for the qualitative analysis of the gross morphology of tissues at the interface of implant and nasal cavity.

2.2.12. Statistical analysis—Average of experimental read out values were collected from all in dependent experiments and final datas were represented as mean ± SEM. Student's t-tests and one way ANOVA with post-hoc Tukey tests were used for comparisons to determine the statistical significance. GraphPad Prism (version 6.01) was used for all statistical analyses with significance set at $p < 0.05$.

3. Results and discussion

3.1. Fabrication of an osmotic core-shell implant specific for BDNF AT delivery using MIND

We have engineered polymeric implants having a unique core-shell architecture as potential candidates for prolonged delivery of different kinds of therapeutics to the CNS using the MIND technique. We have previously established the advantages of MIND technique for *trans*-nasal drug delivery directly to the brain via the basolateral aspect of olfactory epithelium [28]. Herein, we intend to develop biodegradable and biocompatible implants that could sustain-release the entrapped therapeutic payload for increased duration, ultimately yielding enhanced CNS uptake and efficacy, as a complimentary technology to MIND, for CNS delivery of drugs for treatment of various neurodegenerative diseases.

In order to guide the design strategy for such implants, we determined the approximate dimensions of the rat nasal cavity containing the submucosal space formed by the MIND technique to be 1.186 ± 0.08 cm length by 1.131 ± 0.09 cm breadth (Fig. S1). We hypothesized that a core-shell design would be ideal because (1) an osmotic core component encapsulates the payload (e.g., small molecule, biologic, etc.) and modulates its release profile by hydrolytic swelling and (2) an erodible polymeric sheath around the core acts as a barrier layer to delay and further control the drug release profile. Poloxamers or Pluronics are nontoxic and FDA approved amphiphilic high molecular weight polyethylene oxide–polypropylene oxide–polyethylene oxide (PEO–PPO–PEO) triblock copolymers consisting of hydrophilic PEO segments and hydrophobic PPO sections [31,32]. Pluronic F-127-based hydrogels have properties of good water retention, reverse thermal gelation and can also provide controlled release of biomolecules/drugs incorporated within their hydrophilic networks making them good candidates as injectables for drug delivery [33–36]. Several studies highlight the ability of poloxamer-based osmotic membranes to modulate the penetration rate and permeation flux of the corresponding coagulation medium (mostly water) [31,37,38]. Considering these properties, we chose Pluronic F-127 as the core

component entrapping BDNF AT as it could simultaneously behave as an osmotic hydrogel core enhancing the water permeation rate leading to hydrolytic swelling and thereby controlling the rate of AT release. This reported osmotic effect could be regulated with the amount of Pluronic F-127 entrapped in the final implant. PCL, a first generation synthetic aliphatic polyester is an FDA approved non-toxic, biocompatible and biodegradable polymer extensively investigated in the fields of controlled drug delivery and regenerative medicine with a history of human use [39–42]. Herein, we chose PCL as the component for fabricating the outer sheath entrapping Pluronic F-127 core, owing to its hydrophobicity and slower degradation profile using the simple dip-coating technique. The tailorability in processing all properties in addition to the relatively cheaper production strategies, make PCL easily amenable to physical, chemical and biological manipulations to modulate the degradation kinetics in order to suit the specific anatomical site, desired drug release profile and application [39,43–45]. Therefore, the shell is also modular in its biodegradation profile and diffusional kinetics-based release which in turn, is based on the molecular weight of PCL and the sheath thickness. Herein, we engineered PCL shell specifically for diffusional release of the payload (not by degradation) based on the time scale of our overall study.

As the first step, PCL shell in the initial form of a hollow reservoir was fabricated using the method of traditional dip coating (Fig. 1A1–3). An optimized PCL solution concentration of 14% w/vand 9–10 dipping cycles formed a shell with an average thickness of 0.54 ± 0.05 mm and diameter of approximately 5 mm. Concentrated Pluronic F-127 gel with the BDNF AT payload was added to this hollow PCL shell and the open end of the reservoir was subsequently sealed (Fig. 1A4–5). Therefore, the overall strategy offers flexibility with regard to several parameters such as selection of biodegradable polymers or copolymers with different degradation time frames enabling incorporation of a variety of payloads with high loading and control of their release profiles. Processing parameters such as concentration of the polymeric solution, choice of the coating substrate and control of optimum dipping cycles aid in the modulation of dimensions and tailorability of shapes of the implants (Fig. 1A6 and Fig. S2). Specifically, cylindrical PCL shells of different dimensions (~5 mm and ~2 mm) could be fabricated using glass rods as coating substrates with the corresponding diameters (Fig. S2). The qualitative assessment of the surface of PCL coated shell with FESEM revealed a uniform homogenous crack-free morphology and texture (Fig. 1B).

We performed an initial *in vitro* release experiment wherein we assessed the release profile of the fluorescent dye FITC-Dextran entrapped within the implant at different time points until 30 days. This experiment was conducted in order to understand the basic release characteristics of any payload entrapped within the designed implant. FITC-Dextran was chosen owing to its similarity in physico-chemical properties to that of BDNF-AT such as hydrophilicity and molecular weight. We observed a biphasic release profile, with an immediate faster burst release of 2.79 ± 0.13% of the total amount of the entrapped FITC Dextran within 3 h and 3.84 ± 0.18 within 2 days (Fig. 1C). This was followed by a phase of much slower release wherein 4.19 ± 0.2% of the payload was released at day 6 which then increased very slowly to 5.27 ± 0.2% within a span of 30 days (~1.89 fold higher than the release observed at the initial time points). The results also indicated the possibility of obtaining a prolonged release at slower rates for further durations beyond 30 days. We hypothesized that, such a release pattern would ideally mimic the clinical administration of

an initial ‘loading’ bolus dose of the therapeutic payload in the beginning of the proposed treatment period in patients, followed by a trend of slower release for ‘maintenance therapy’. Such a strategy would obviate the need for repeated drug administrations and also enhance the pharmacokinetic advantages in contrast to single phase extended formulations [46,47]. It is also important to note that the rate at which drug release occurs in different phases of the biphasic profile can be controlled upon modulating the formulation parameters such as concentration of the Pluronic F-127 gel core and the design attributes of the PCL polymeric sheath. Hence, the engineering of core-shell implants was established to be a simple yet versatile approach offering good control over implant dimensions as well as an optimal drug release profile; the two important characteristics for MIND implants.

3.2. In vivo administration of BDNF AT core-shell implants using MIND

Core-shell implants entrapping BDNF AT as payload were implanted within the submucosal space of healthy Sprague Dawley rats using the MIND technique. The clinical MIND procedure in humans requires a simple endoscopy guided *trans*-nasal injection of drug within the olfactory sub-epithelium in awake, topically anesthetized patients. In contrast, the rat snout is too small to access this space *trans*-nasally thereby necessitating an open surgical approach [28].

The sagittal midline skin incision simultaneously exposes the rat nasal bones while creating the subcutaneous pocket to accept the implant (Fig. 2A). Careful drilling of a segment of the nasal bones exposes the intact olfactory submucosa (Fig. 2B) onto which the core shell implant was placed (Fig. 2C). The implant dimensions were designed to conform to this cavity without compressing the surrounding structures which also mitigated the need for suturing them. Primary closure of the surgical incision by continuous suturing (Fig. 2D) facilitated rapid wound closure without signs of infection or dehiscence (Fig. S3). The MIND implantation procedure easily reproducible and all experimental rats remained healthy throughout the study period of 4 weeks without any signs of illness or lethargy.

3.3. CNS delivery of BDNF AT via MIND implantation and pharmacokinetic analysis

The entire *in vivo* study was conducted over a time span of 4 weeks with time points of 4, 7, 14, 21 and 28 days post implantation to assess the long term BDNF AT delivery potential of MIND implants. Animals were euthanized at each time point and AT levels in different subregions of brain were quantified to analyse the CNS uptake and brain distribution of BDNF ATs. The sub-regions chosen for our study were olfactory bulb (OB); the first intracranial structure present in the *trans*-olfactory route, striatum (STR) in the forebrain, hippocampus (HC) which forms an extension of the temporal part of cerebral cortex, substantia nigra (SN) in the midbrain and cerebellum (CB) in the hindbrain [48,49]. The sustained BDNF AT distribution over all these different sub regions of brain over 28 days can be noted from Fig. 3..

The observed trends in mean AT concentration over time indicate a tissue-specific AT distribution pattern, which is in line with prior observations for the CNS distribution of AT [28]. For OB, the highest mean AT concentrations were detected on day 4 (~1.8 pg/μg) which was then followed by a slow and steady decline in the AT levels over time. We

observed that the BDNF AT levels persisted in the OB at detectable concentrations for the duration of the study. A similar trend was also noted for the striatum (STR) wherein the mean AT levels decreased over time. However, the hippocampus (HC) and substantia nigra (SN) displayed a different trend wherein high mean AT levels were observed on day 7 (1.25–1.5 pg/μg) which was then followed by a steep decline to negligible AT amounts. Although the cerebellum (CB) displayed a similar trend in AT concentration to the HC and SN, the overall concentration was higher, and therefore appreciable AT levels were detectable at later timepoints. These data suggest that the midbrain and hindbrain sub-regions displayed comparable trends of AT distribution with a slower rise in mean AT levels and a subsequent decrease towards 2–4 weeks.

Furthermore, no AT was detected in plasma samples of all animals subjected to MIND implantation, which again confirms our previous observation [28] that MIND mediated CNS uptake occurs directly through the olfactory epithelium and not by secondary peripheral distribution [50,51].

We further characterized the time course of BDNF AT tissue concentrations using NCA to evaluate pharmacokinetic parameters of the implant formulation (Table 1). These data also suggest tissue-specific distribution of AT within the CNS. The extent of distribution, as determined by AUC values, varied from 115 to 369 pg*mL^{-1}*day, with the least distribution in the HC and SN, and the most AT distributed to the OB (Table 1). Similar trends were observed for C_{max} with a range of 13.4–19.4 pg*mL^{-1} for deep brain tissues and 27.8 pg*mL^{-1} for the OB. Interestingly, MRT values, which ranged from 7.27 to 10.8 days, were more uniform for all brain sub-regions which indicates that on average, AT molecules stayed in the brain for more than a week and were cleared from tissue sub-regions at similar rates. Collectively, these pharmacokinetic parameters suggest that the OB, which is the tissue closest to the implant site and also the first point of contact in the *trans*-olfactory route [48], behaved distinctly from deeper brain tissues. The rate of AT diffusion partly enhanced by the swelling and osmotic action of Pluronic F127 gel core could have also led to high AT distribution into OB.

Overall the PK studies confirmed that MIND implants could elute BDNF AT for prolonged durations thereby successfully delivering the otherwise BBB-impermeant AT to deep brain sub regions and sustaining its concentrations for extended time periods.

3.4. BDNF protein levels in brain sub-regions at different time points post MIND implantation

Having analyzed the PK profiles and CNS distribution of BDNF AT delivery by MIND implants, we next studied its biological effects by quantifying the BDNF protein levels in brain subregions (Fig. 4) and assessing the response kinetics (Table 2). Previous studies have established the age-dependent significant variations in BDNF distribution and expression levels in different regions of rat brain [52–54]. Therefore, it was crucial for us to consider aging of MIND implanted rats within the treatment frame of 28 days as a study parameter. Therefore, naïve rats of appropriate ages and matched sexes were used as negative controls for this study (Fig. 4).

Within 2 weeks post MIND implantation, we noticed significant BDNF upregulation in all tissues in comparison to naïve BDNF levels as shown in Fig. 4A. A 2-fold increment in BDNF expression was observed at days 4 and 7 in OB relative to naïve BDNF levels. By day 14, BDNF levels in the OB were 4-fold higher than naïve animals, which was a statistically significant difference. Similarly, the STR, SN, and HC all demonstrated statistically significant increases in BDNF levels at 4, 7, and 14 days. There were tissue-specific BDNF level increases of 2.5–3.5 fold in STR and SN and 3–4 fold increases in the HC. The BDNF expression at day 14 was the highest in all of these tissues compared to the levels attained at days 4 and 7. The CB was the only region wherein a slightly different trend was noted with a plateau in BDNF levels from days 4–14. We did not notice upregulation of BDNF levels at day 21 (Fig. 4B) or day 28 (Fig. 4C) relative to the corresponding naïve levels. This observation could be correlated to the extended period of very low BDNF AT levels noted in majority of the brain sub-regions at these time points. Additionally, it can also be attributed to the reported fluctuations in BDNF levels in the course of rat brain development and aging. Semba et al. has previously quantified the specific changes in BDNF concentrations in different regions of rat brain in the course of its development and aging for ~6 months [53]. While regions such as olfactory bulb, hippocampus and cerebellum clearly indicated a steady increase in BDNF levels in the course of aging until 60–120 days, regions such as cerebral cortex, hypothalamus and striatum exhibited an opposite oscillating trend of an increase followed by a steep decrease around the same time frame. These findings also underline the broad and differential expression of BDNF mRNA throughout the adult brain. This stands in contrast to other neurotrophins, such as NT-3, with much narrower and limited mRNA distribution which makes BDNF more susceptible to intricate variations under different treatment conditions [55–59]. To further probe these findings, we also included animals implanted with bare or placebo core-shell implants (without BDNF-AT) as an additional negative control for the extended time point of 28 days and compared their BDNF levels to those of rats of comparable age group (Fig. S4). We noted that there was no increase in BDNF levels with the placebo implant. While there were no statistical differences between the BDNF levels of olfactory bulb and cerebellum of implant bearing rats relative to their respective controls, other tissues showed a 0.2–0.3 fold decrease, further highlighting the need and importance of BDNF AT to induce BDNF protein upregulation.

To further evaluate the outcomes associated with the novel implant formulation, the kinetics of the BDNF response were also evaluated via NCA (Table 2). This analysis suggests that the BDNF response kinetics behave somewhat similarly amongst the brain tissues, irrespective of distance from the implant site. Indeed, C_{max} values ranged from 1.01 to 1.35 pg*μg protein^{-1} for all brain tissues (Table 2). Moreover, the AUEC values, which represent the extent of BDNF response over this time-frame, ranged from 13.8 to 18.9 pg*μg protein^{-1}*day.

Collectively, the kinetic parameters describing the BDNF response suggest that there are tissue-specific responses to BDNF-AT exposure that are not directly proportional to AT exposure. These findings reaffirm the previously observed lack of a direct PK/PD relationship for BDNF AT [28]. The tissue-specific amounts of BDNF mRNA and variable BDNF NAT copy numbers strongly influence the extent of BDNF upregulation induced

by the inhibition of BDNF-AS by AT binding, mechanisms which support an indirect PK/PD response for the BDNF AT [17, 60]. Moreover, these findings indicate that future PK/PD modeling of BDNF AT will require special considerations including region-, age-, and species-specific variations in response. These nuances of the BDNF response present a challenge for animal to human allometric scaling, and therefore extra care must be taken with model validation to account for the anticipated variabilities in response.

3.5. Comparison of kinetics of BDNF AT delivery and BDNF protein response for the AT-implant relative to AT-Gel depot

Having established the sustained AT delivery potential of core-shell implants, we evaluated the performance of the implants by comparing the data with that of the AT-Gel (BDNF AT dispersed in Pluronic-F127 gel; same AT dose of 0.15 mg/kg) reported previously by our group [28] (Fig. 5). Given the additional complexity of the core-shell implant formulation, relative to the AT-Gel, it was critical to establish the relative delivery efficiency of the novel formulation and therefore discern the value added. Our previously reported AT-Gel depot data from 0 to 96 h [28] was utilized for this comparison since the terminal data points were at or under the limits of detection, and any later time points were expected to give non-quantitative results. Using NCA data for both formulations, the C_{max}, MRT and AUC or AUEC ratios were calculated for the MIND implant relative to the MIND depot, for both AT (Fig. 5A–D) and BDNF protein levels (Fig. 5E–G).

As shown in Fig. 5A, the implant formulation substantially reduced the C_{max} in the OB and reduced the tissue-to-tissue variability in C_{max}, relative to the depot formulation. As shown in Fig. 5B, the implant formulation substantially increased the exposure in all tissues, as measured by AUC, when compared to the AT-gel depot. Indeed, exposure in the deep brain tissues of interest, such as the HC, SN, and CB, showed a remarkable 1000% increase. Exposure in the OB was only increased by 300%, which suggests that the implant formulation increased the fraction of the dose reaching the end target regions in addition to increasing overall exposure relative to the gel depot. In addition to increasing the extent of exposure, the implant formulation greatly increased the duration of exposure as determined by MRT (Fig. 5C), with tissue-specific increases ranging from nearly 1000% in the OB and STR to over 2500% in the CB. Collectively, these changes in peak and cumulative exposure (Fig. 5D) suggest that the implant formulation was able to flatten and extend the AT concentration-time curve and thereby enhance the delivery efficiency of an equivalent AT dose when compared to the gel depot.

A comparison of the kinetics of the BDNF response shows that the implant formulation increased the BDNF C_{max} relative to the depot (Fig. 5E), which stands in contrast to the effect seen on AT C_{max}. The maximum BDNF concentration in the OB increased by nearly 250% for animals treated with the implant formulation, which suggests that the BDNF response is not driven by the AT C_{max}. Interestingly, the C_{max} of the BDNF response did not change substantially for deep brain tissues in animals implanted with MIND core-shell implants. As shown in Fig. 5F, treatment with MIND core-shell implants substantially increased the cumulative BDNF exposure, as determined by the AUEC, by nearly 1000% in all tissues when compared to the depot formulation. The changes in BDNF response kinetics

for the implant relative to the depot (Fig. 5G) demonstrate that the novel formulation was able to substantially extend the cumulative BDNF exposure for the same dose of BDNF-AT. The observed differences in exposure to AT and BDNF suggest differences in the intrinsic tissue response to AT, likely due to tissue-specific differences in BDNF mRNA levels and/or BDNF NAT levels [17,60].

3.6. Analysis of explants for residual BDNF AT

Implants retrieved from the surgery sites upon rat sacrifice (Fig. 6A) at different time points (Fig. S5) were weighed and thereafter cut open to withdraw the remnant gel volumes (Fig. 6B). Any potential change to the integrity of implants in the course of *in vivo* implantation would have significantly hampered the ease and success of explanting them out of the nasal cavities. However, all the implants could be easily explanted at all time points and they were found to preserve their original shape without distinct changes in morphology (Fig. S4) and mechanical integrity (no crimpling or tearing). An increase in the volume of core was noted for implants retrieved at late time points (Fig. S4). Fig. 6C shows the percent change in implant weights and remnant gel volumes. As evident from the figure, implants of the initial time points displayed a slight decrease in weights which was then followed by an increase within 14 days, when compared to the weights of implants preimplantation. A 20% increase in weight was noted around 21 and 28 days. Similarly, the remnant gel volume collected from implants at initial time point was smaller than the ones from longer time points such 21 and 28 days. This could be attributed to the mechanism of diffusion which favored the release of BDNF AT from the core to the rat submucosal space. However, with the progression of time, the Pluronic F-127 gel core also enhanced the permeation rate of biological fluid present in the vicinity of implant due to an osmotic action and contributed to the increase in the weight of implant as well as the gel volume at longer time points (also seen in implants of late time points in Fig. S5).

The remnant AT amounts in retrieved gel fractions were analyzed and compared to the initially loaded AT amounts to compute the *in vivo* cumulative AT release% (Fig. 6D). It was observed that ~30% of BDNF AT was released from the implant *in vivo* within the first few days which increased to ~45% by 1 week and 50% by 2nd week. The slow release rate of AT after day 4 also emphasizes the role of diffusion as the prominent mechanism at the initial time points and can also be related to the higher BDNF AT levels detected in brain regions at these time points (Fig. 3A). However, the rate of AT release post 2 weeks could have slowed down due to the compounded effects of water permeation into the core matrix. We noted a cumulative AT release of ~50–60% from implants explanted at week 3, which strongly indicates the possibility of further release (of the remaining 40%) gradually over time. However, we could not extract the accurate gel fraction from the 28th day implants, as there were higher amounts of transudates mixed with the gel which subsequently interfered with the sample processing and remnant AT analysis. The smaller fraction of BDNF AT released in the longer time points can also be correlated to the relatively lower amounts of BDNF AT detected in the deeper brain tissues at these timepoints (Fig. 3). This also emphasizes the utility of such implants as drug depots favoring slower yet sustained release profiles.

We also evaluated the surface morphology of all explanted implants qualitatively by FESEM (Fig. S6). The changes to the implant morphology at day 4 were minimal except for the coarse surface topography and enhanced roughness relative to pre-implanted ones (Fig. 1B) which is expected to happen in the course of contact with a biological fluid/surgery site. The implant surface at day 7 showed small pore-like structures which could have possibly formed along the course of the matrix hydration. The surface at day 28 showed the presence of small cracks or crevices which are typical characteristics of the onset of polymer degradation or erosion [61,62]. These observations suggest the possibility of polymer degradation becoming the dominant release mechanism at later timepoints instead of diffusion. Although PCL has a slow biodegradation profile, the surrounding biological milieu with the exposure to transudates and enzymes at the site of surgical implantation, and enhanced rate of water permeation triggered by the osmotic core could have accelerated its hydrolytic and enzymatic degradation profile [63,64].

3.7. Histological evaluation of rat nasal tissues after MIND implantation procedure

The current study was carried out for an extended period of 28 days and hence it was imperative to evaluate the long-term safety of the procedure as well as biocompatibility of the core-shell implants. We have previously established the safety of MIND approach in naïve Sprague Dawley rats [28]. As mentioned above, the animals remained healthy throughout the treatment period of 28 days without any significant changes in their routine activities or behavior. Upon euthanasia at different time points, the implantation site within the rat submucosal space was carefully inspected to check for any visual signs of inflammation, tissue ingrowth or fibrous capsule formation around the implant which are the commonly observed signs of foreign body reaction [65, 66]. As shown in Fig. S7, there were no abnormalities in the rat nasal cavities or any prominent signs of infection or tissue ingrowth. Further, we collected the tissues from the interface of implant and nasal cavity to qualitatively assess these signs by standard histological analysis (Fig. 7). Apart from a slightly thickened epidermis observed at the initial few time points which is expected as the response to the surgical incision, there were no significant changes in the tissue histology of implanted animals relative to the intact histology of untreated animals. The absence of any prominent histological signs of adverse tissue reactions confirmed the biocompatibility of the fabricated core-shell implants.

4. Conclusions

The present study demonstrates the development and application of biodegradable implants with a unique osmotic core and polymeric shell design as a potential strategy to prolong delivery of BBB impermeant biological therapeutics to the CNS via the MIND technique. Using a straightforward implant fabrication followed by MIND implantation procedure, we demonstrate evidence of sustained release and delivery of the therapeutic to specific regions in Sprague-Dawley rat brain. The implant composition and dimensions can be tailored for specific therapeutic payloads and indications.

In the context of BDNF AT delivery, an osmotic Pluronic F-127 gel core entrapping BDNF AT and a PCL dip-coated sheath enables the modulation and optimal control of

the release of AT over sustained duration as compared to the previously reported gel depot [28]. Such implants resulted in a more efficient and prolonged CNS uptake of BDNF AT relative to previously repored gel formulations of BDNF AT. We observed a substantial 1000% enhancement in the cumulative BDNF exposure for animals administered with the MIND implant, particularly in regions such as hippocampus and substantia nigra, which are important for AD and PD therapy. Therefore, the core shell implant technology coupled with MIND approach can synergistically serve to improve the CNS uptake and prolonged delivery of therapeutics to the brain for extended time periods. The MIND dechnique is directly derived from routine, minimally invasive, non-surgical Ear, Nose and Throat (ENT) clinic procedures and the implant fabrication is fairly simple and flexible. Consequently, the resulting combined MIND Implant approach may be directly clinically translated for the treatment of chronic age-related neurodegenerative diseases such as Alzheimer's and Parkinson's disease.

Supplementary Material

Refer to Web version on PubMed Central for supplementary material.

Acknowledgements

The authors acknowledge the assistance provided by William Fowle at the Electron Microscopy Center, Northeastern University (Boston, MA) for performing FESEM of the implant samples and Biania Fan and Philip Seifert at the SERI Morphology Core, Schepens Eye Research Institute of Massachusetts Eye and Ear Infirmary (Boston, MA) for the assistance provided with the hematoxylin and eosin (H&E) staining.

Funding statement

The research work presented in this manuscript was supported by National Institute of Neurological Disorders and Stroke (NINDS) of the National Institutes of Health (NIH) under award number R01-NS108968-01. The content is solely the responsibility of the authors and does not necessarily represent the official views of the National Institutes of Health.

Data availability

Data associated with the studies described in this manuscript will be available upon request.

List of abbreviations

AD	Alzheimer's Disease
AT	AntagoNAT
AUC	Area under the curve
AUEC	Area under the effect curve
AUMC	Area under the first moment curve
BBB	Blood-brain barrier
BDNF	Brain derived neurotrophic factor
C_{max}	Maximum concentration

CNS	Central nervous system
CSF	Cerebrospinal Fluid
ENT	Ear, Nose and Throat
FESEM	Field Emission Scanning Electron Microscopy
FITC	Fluorescein isothiocyanate
ICV	Intracerebroventricular
IT	Intrathecal
MIND	Minimally Invasive Nasal Depot
MRT	Mean residence time
NAT	Natural antisense transcript
NCA	Noncompartmental analysis
OE	Olfactory epithelium
PCL	Poly(epsilon-caprolactone)
PD	Parkinson’s disease
(PEO–PPO–PEO)	Polyethylene oxide–polypropylene oxide–polyethylene oxide
$\mathbf{t_{max}}$	Time of maximum concentration
2,2,2-TFE	2,2,2-Trifluoroethanol

References

[1]. Andreone BJ, Larhammar M & Lewcock JW Cell Death and Neurodegeneration. vol. 19.

[2]. Farooqui AA, Chapter 1-classification and molecular aspects of neurotraumatic diseases: similarities and differences with neurodegenerative and neuropsychiatric diseases, in: Farooqui AA (Ed.), Ischemic and Traumatic Brain and Spinal Cord Injuries, 1–40, Academic Press., 2018.

[3]. Giacalone Marilù, Filippo Di Sacco Ippolito Traupe, Pagnucci Nicola, Forfori Francesco, Giunta Francesco, Chapter 2 - blueberry polyphenols and neuroprotection, in: Bioactive Nutraceuticals and Dietary Supplements in Neurological and Brain Disease, Watson Ronald Ross, Preedy Victor R., 2015, pp. 17–28. Academic Press.

[4]. Sheikh S, Safia Haque E, Mir SS, Neurodegenerative diseases: multifactorial conformational diseases and their therapeutic interventions, J. Neurodegener. Dis (2013) 1–8, 2013.

[5]. Przedborski S, Vila M, Jackson-Lewis V, Neurodegeneration: what is it and where are we? J. Clin. Invest 111 (2003) 8.

[6]. Duggan M, Torkzaban B, Ahooyi TM, Khalili K, Gordon J Age-related neurodegenerative diseases. J. Cell. Physiol 235 (2020) 3131–3141. [PubMed: 31556109]

[7]. Tanner CM, Goldman SM, Epidemiology of Parkinson’s Disease, vol. 20, 1996.

[8]. Huang EJ, Reichardt LF, Neurotrophins: roles in neuronal development and function, Annu. Rev. Neurosci 24 (2001) 677–736. [PubMed: 11520916]

[9]. Padmakumar S, Taha MS, Kadakia E, Bleier BS, Amiji MM, Delivery of neurotrophic factors in the treatment of age-related chronic neurodegenerative diseases, Expet Opin. Drug Deliv 17 (2020) 323–340.

[10]. Bathina S, Das UN, Brain-derived neurotrophic factor and its clinical implications, Arch. Med. Sci 6 (2015) 1164–1178.

[11]. Miranda M, Morici JF, Zanoni MB, Bekinschtein P, Brain-derived neurotrophic factor: a key molecule for memory in the healthy and the pathological brain, Front. Cell. Neurosci 13 (2019) 363. [PubMed: 31440144]

[12]. Parain K et al. Reduced Expression of Brain-Derived Neurotrophic Factor Protein in Parkinson's Disease substantia nigra. 5.

[13]. Palasz E, et al. , BDNF as a promising therapeutic agent in Parkinson's disease, Int. J. Mol. Sci 23 (2020).

[14]. Mogi M, et al. , Brain-derived growth factor and nerve growth factor concentrations are decreased in the substantia nigra in Parkinson's disease, Neurosci. Lett 4 (1999).

[15]. Murer MG, Yan Q, Raisman-Vozari R, Brain-derived neurotrophic factor in the control human brain, and in Alzheimer's disease and Parkinson's disease, Prog. Neurobiol 63 (2001) 71–124. [PubMed: 11040419]

[16]. Zigova T, Pencea V, Wiegand SJ, Luskin MB, Intraventricular administration of BDNF increases the number of newly generated neurons in the adult olfactory bulb, Mol. Cell. Neurosci 11 (1998) 234–245. [PubMed: 9675054]

[17]. Modarresi F, et al. , Inhibition of natural antisense transcripts in vivo results in gene-specific transcriptional upregulation, Nat. Biotechnol 30 (2012) 453–459. [PubMed: 22446693]

[18]. Kowiański P, et al. , BDNF: a key factor with multipotent impact on brain signaling and synaptic plasticity, Cell. Mol. Neurobiol 38 (2018) 579–593. [PubMed: 28623429]

[19]. Mitchelmore C, Gede L, Brain derived neurotrophic factor: epigenetic regulation in psychiatric disorders, Brain Res 1586 (2014) 162–172. [PubMed: 25223903]

[20]. Mercado N, Collier T, Sortwell C, Steece-Collier K, BDNF in the Aged Brain: Translational Implications for Parkinson's Disease, vol. 18, 2018.

[21]. Cattaneo A, Cattane N, Begni V, Pariante CM, Riva MA, The human BDNF gene: peripheral gene expression and protein levels as biomarkers for psychiatric disorders, Transl. Psychiatry 6 (2016) e958. [PubMed: 27874848]

[22]. Martínez-Levy GA & Cruz-Fuentes CS Genetic and Epigenetic Regulation of the Brain-Derived Neurotrophic Factor in the Central Nervous System. vol. 14.

[23]. Khorkova O, Wahlestedt C, Oligonucleotide therapies for disorders of the nervous system, Nat. Biotechnol 35 (2017) 249–263. [PubMed: 28244991]

[24]. Smith RA et al. Antisense Oligonucleotide Therapy for Neurodegenerative Disease. vol. 8.

[25]. Cohen-Pfeffer JL, et al. , Intracerebroventricular delivery as a safe, long-term route of drug administration, Pediatr. Neurol 67 (2017) 23–35. [PubMed: 28089765]

[26]. Slavc I, et al. , Best practices for the use of intracerebroventricular drug delivery devices, Mol. Genet. Metabol 124 (2018) 184–188.

[27]. Hanson LR, Frey WH, Intranasal delivery bypasses the blood-brain barrier to target therapeutic agents to the central nervous system and treat neurodegenerative disease, BMC Neurosci 9 (2008) S5.

[28]. Padmakumar S, et al. , Minimally invasive nasal depot (MIND) technique for direct BDNF AntagoNAT delivery to the brain, J. Contr. Release 331 (2021) 176–186.

[29]. DiResta GR, et al., Measurement of brain tissue density using pycnometry, in: Reulen H-J, Baethmann A, Fenstermacher J, Marmarou A, Spatz M (Eds.), Brain Edema VIII, vols. 34–36, Springer Vienna, 1990, 10.1007/978-3-7091-9115-6_12.

[30]. Noncompartmental Analysis - MATLAB & Simulink. (2017).

[31]. Lv C, et al. , Enhanced permeation performance of cellulose acetate ultrafiltration membrane by incorporation of Pluronic F127, J. Membr. Sci 7 (2007).

[32]. Falath W, Sabir A, Jacob KI, Highly Improved Reverse Osmosis Performance of Novel PVA/DGEBA Cross-Linked Membranes by Incorporation of Pluronic F-127 and MWCNTs for Water Desalination, 2016, p. 14.

[33]. Tan H, Marra KG, Injectable, biodegradable hydrogels for tissue engineering applications, Materials 3 (2010) 1746–1767.

[34]. Gioffredi E, et al. , Pluronic F127 hydrogel characterization and biofabrication in cellularized constructs for tissue engineering applications, Procedia CIRP 49 (2016) 125–132.

[35]. Gilbert JC, Hadgraft J, Bye A, Brookes LG, Drug release from Pluronic F-127 gels, Int. J. Pharm 32 (1986) 223–228.

[36]. Guzmán M, García FF, Molpeceres J, Aberturas MR, Polyoxyethylene-polyoxypropylene block copolymer gels as sustained release vehicles for subcutaneous drug administration, Int. J. Pharm 80 (1992) 119–127.

[37]. Iwasaki Y, Platelet compatible blood filtration fabrics using a phosphorylcholine polymer having high surface mobility, Biomaterials 24 (2003) 3599–3604. [PubMed: 12809789]

[38]. Ishihara K, Hanyuda H & Nakabayashi N Synthesis of Phospholipid Polymers Having a Urethane Bond in the Side Chain as Coating Material on Segmented Polyurethane and Their Platelet Adhesion-Resistant Properties. vol. 7.

[39]. Woodruff MA, Hutmacher DW, The Return of a Forgotten Polymer—Polycaprolactone in the 21st Century, 2010, p. 40.

[40]. Manoukian OS, et al., Biodegradable Polymeric Injectable Implants for Long-Term Delivery of Contraceptive Drugs, vol. 23, 2019.

[41]. Boia R, et al. , Porous poly(ε-caprolactone) implants: a novel strategy for efficient intraocular drug delivery, J. Contr. Release 316 (2019) 331–348.

[42]. Holländer J, et al. , Three-dimensional printed PCL-based implantable prototypes of medical devices for controlled drug delivery, J. Pharmacol. Sci 105 (2016) 2665–2676.

[43]. Malikmammadov E, Tanir TE, Kiziltay A, Hasirci V, Hasirci N, PCL and PCL-based materials in biomedical applications, J. Biomater. Sci. Polym. Ed 29 (2018) 863–893. [PubMed: 29053081]

[44]. Arakawa CK, DeForest CA, Polymer design and development, in: Biology and Engineering of Stem Cell Niches, Elsevier, 2017, pp. 295–314, 10.1016/B978-0-12-802734-9.00019-6.

[45]. Guarino V, Gentile G, Sorrentino L, Ambrosio L, Polycaprolactone: synthesis, properties, and applications: polycaprolactone: synthesis, properties, and applications, in: Encyclopedia of Polymer Science and Technology, John Wiley & Sons, Inc.) 1–36 (John Wiley & Sons, Inc., 2017, 10.1002/0471440264.pst658.

[46]. Dingemanse J, Kleinbloesem CH, Ch Crevoisier G Lankhaar, U.E. Gasser, Pharmacokinetic studies with a dual-release formulation of levodopa, a novel principle in the treatment of Parkinson’s disease, Eur. Neurol 39 (1998) 119–124. [PubMed: 9520073]

[47]. Amjad F, et al. , Current practices for outpatient initiation of levodopa-carbidopa intestinal gel for management of advanced Parkinson’s disease in the United States, Adv. Ther 36 (2019) 2233–2246. [PubMed: 31278691]

[48]. Shantha TR, Bypassing the BBB: drug delivery from the olfactory mucosa to the CNS, Drug Dev 17 (2017) 7.

[49]. Watson C, Kirkcaldie M, A Map of the Brain - Chapter 3, In : the Brain, in: Watson Charles, Kirkcaldie Matthew, Paxinos George (Eds.), Academic Press, 2010, pp. 25–42.

[50]. Harkema JR, Carey SA, Wagner JG, The Nose revisited: a brief review of the comparative structure, function, and toxicologic pathology of the nasal epithelium, Toxicol. Pathol 34 (2006) 252–269. [PubMed: 16698724]

[51]. Gänger S, Schindowski K, Tailoring formulations for intranasal nose-to-brain delivery: a review on architecture, physico-chemical characteristics and mucociliary clearance of the nasal olfactory mucosa, Pharmaceutics 10 (2018) 116.

[52]. Silhol M, Bonnichon V, Rage F, Tapia-Arancibia L, Age-related changes in brain-derived neurotrophic factor and tyrosine kinase receptor isoforms in the hippocampus and hypothalamus in male rats, Neuroscience 132 (2005) 613–624. [PubMed: 15837123]

[53]. Katoh-Semba R & Takeuchi IK Distribution of Brain-Derived Neurotrophic Factor in Rats and its Changes with Development in the Brain. vol. 9.

[54]. Coria-Lucero CD Rhythmic Bdnf and TrkB expression patterns in the prefrontal cortex are lost in aged rats. Brain Res. 8.

[55]. Conner JM, Lauterborn JC, Yan Q, Gall CM & Varon S Distribution of brain-derived neurotrophic factor (BDNF) protein and mRNA in the normal adult rat CNS: Evidence for Anterograde Axonal Transport. 19.

[56]. Castren E, Thoenen H, Lindholm D, Brain-derived neurotrophic factor messenger RNA is expressed in the septum, hypothalamus and in adrenergic brain stem nuclei of adult rat brain and is increased by osmotic stimulation in the paraventricular nucleus, Neuroscience 64 (1995) 71–80. [PubMed: 7708216]

[57]. Guthrie KM, Gall CM, Differential expression of mRNAs for the NGF family of neurotrophic factors in the adult rat central olfactory system, J. Comp. Neurol 313 (1991) 95–102. [PubMed: 1761757]

[58]. Ceccatelli S, Ernfors P, Villar MJ, Persson H, Hokfelt T, Expanded distribution of mRNA for nerve growth factor, brain-derived neurotrophic factor, and neurotrophin 3 in the rat brain after colchicine treatment, Proc. Natl. Acad. Sci. Unit. States Am 88 (1991) 10352–10356.

[59]. Phillips H, Hains J, Laramee G, Rosenthal A, Winslow J, Widespread expression of BDNF but not NT3 by target areas of basal forebrain cholinergic neurons, Science 250 (1990) 290–294. [PubMed: 1688328]

[60]. Mazur C, et al. , Brain pharmacology of intrathecal antisense oligonucleotides revealed through multimodal imaging, JCI Insight 4 (2019), e129240.

[61]. Visan AI, et al. , Long-term evaluation of dip-coated PCL-blend-PEG coatings in simulated conditions, Polymers 12 (2020) 717.

[62]. Lyu JS, Lee J-S, Han J, Development of a biodegradable polycaprolactone film incorporated with an antimicrobial agent via an extrusion process, Sci. Rep 9 (2019) 11. [PubMed: 30626904]

[63]. Bartnikowski M, Dargaville TR, Ivanovski S, Hutmacher DW, Degradation mechanisms of polycaprolactone in the context of chemistry, geometry and environment, Prog. Polym. Sci 96 (2019) 1–20.

[64]. Andhariya JV, et al. , Development of Level A in vitro-in vivo correlations for peptide loaded PLGA microspheres, J. Contr. Release 308 (2019) 1–13.

[65]. Nayyer L, Jell G, Esmaeili A, Birchall M, Seifalian AM, A biodesigned nanocomposite biomaterial for auricular cartilage reconstruction, Adv. Healthc. Mater 5 (2016) 1203–1212. [PubMed: 26992039]

[66]. Atlan Michael, Nuti Gina, Wang Hongpeng, Decker Sherri, Perry TracyAnn, Breast implant surface texture impacts host tissue response, J. Mech. Behav. Biomed. Mat (2018) 377–385.

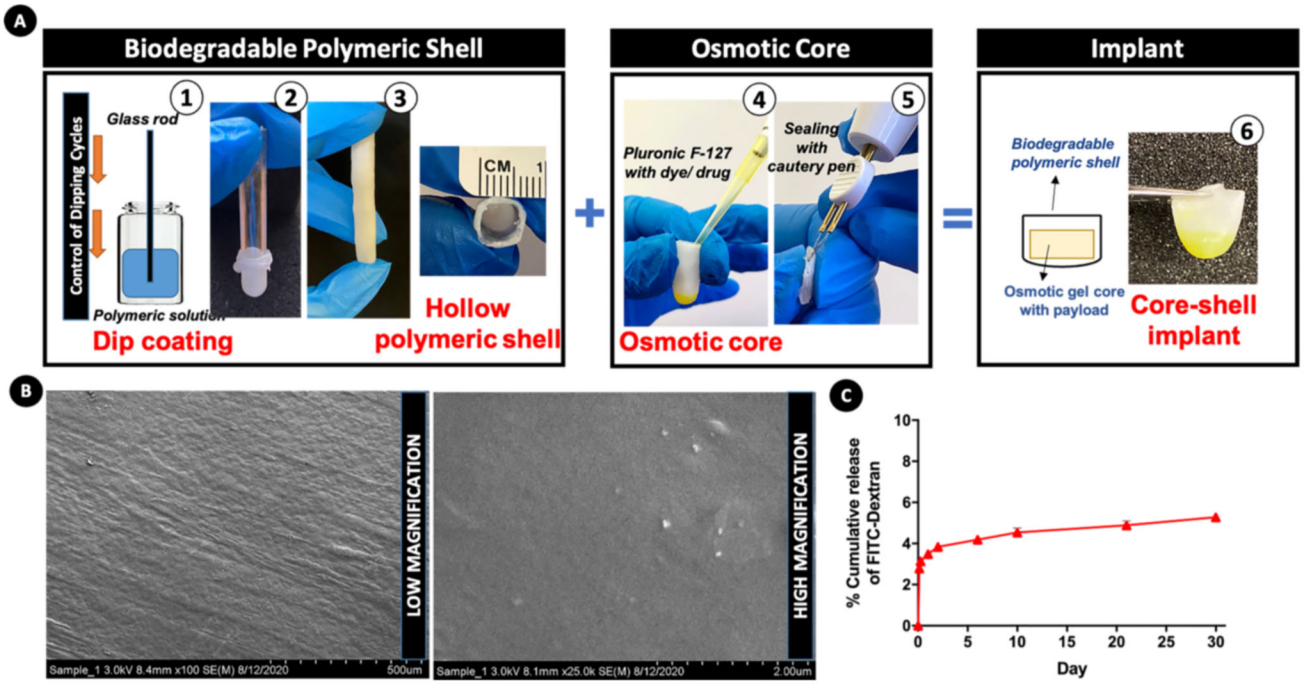

Fig. 1.

Design and fabrication strategy of osmotic core-shell implant. (A) Fabrication of biodegradable polymeric shell: (1) a lubricated cylindrical glass rod acting as the coating substrate is dipped into a concentrated PCL-TFE solution for 9–10 cycles and vacuum dried; (2) the PCL shell is peeled off from the substrate rod such that it forms a (3) hollow reservoir; (4) Pluronic F-127 solution with the dye/drug corresponding to *in vivo* dose is pipetted into the hollow shell; (5) the shell is then shortened and its open end is sealed with heat using cautery pen; (6) the final implant, composed of an osmotic core entrapping the payload enclosed within a biodegradable shell. (B) Surface morphology of dip-coated PCL shell assessed by FESEM (low and high magnification images). (C) In vitro cumulative release of FITC-dextran dye (expressed as percent of the total payload) from the implant into PBS (37 °C, pH 7.4, 100 rpm).

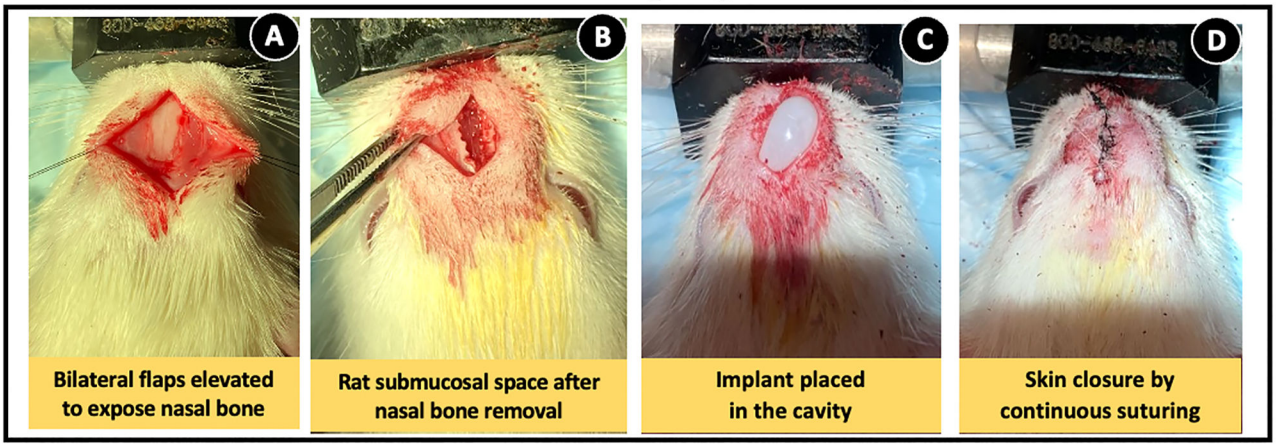

Fig. 2. *In vivo* administration of BDNF AntagoNAT (AT) core-shell implant by MIND technique to the submucosal space of naïve Sprague Dawley rats.

(A) Exposure of nasal bones after the elevation of bilateral skin flaps post-midline sagittal incision. (B) High speed drill-aided removal of nasal bone for formation of a subcutaneous cavity within the submucosal space. (C) Placing BDNF AT core-shell implant within the cavity. (D) Closure of skin incision with nylon sutures.

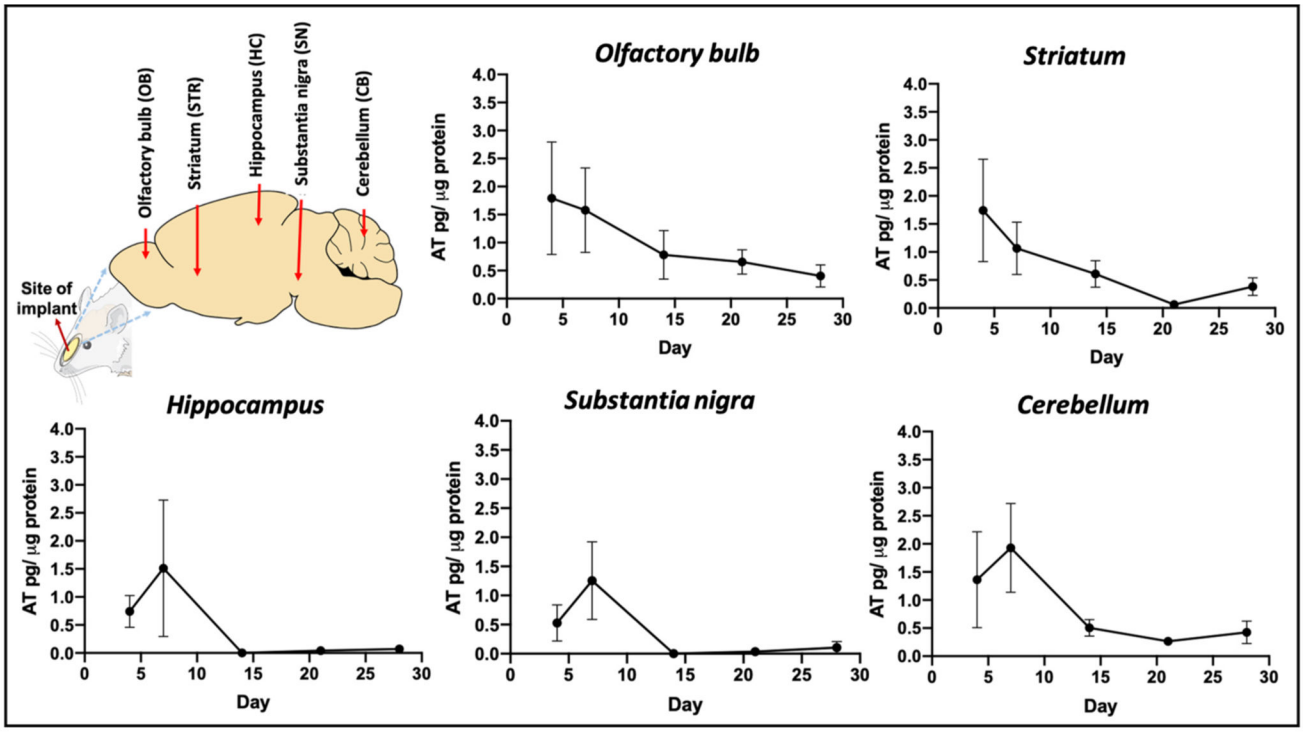

Fig. 3. BDNF AntagoNAT (AT) levels in rat brain sub-regions at different time points post-MIND implantation.

Illustration showing the location of implant with various sub-regions of interest in rat brain and BDNF AT levels in these tissues at different time points such as 4, 7, 14, 21 and 28 days, quantified by BDNF AT hybridisation assay (n = 4 rats/time point, AT levels represented as mean ± SEM).

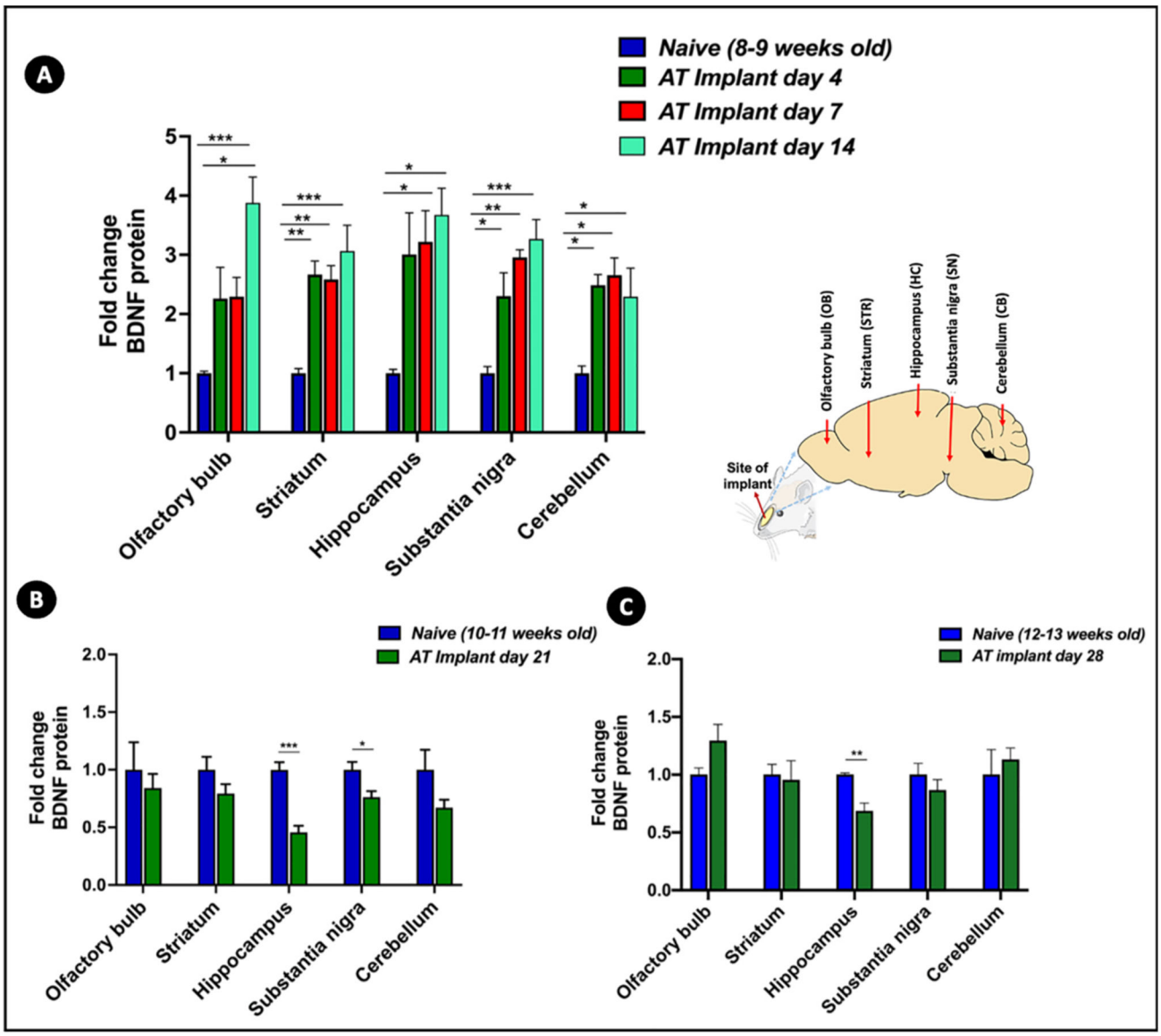

Fig. 4. BDNF protein levels in rat brain sub-regions at different time points post-MIND implantation.

BDNF protein levels in brain sub-regions of rats administered via MIND implants at different time points such as (A) 4, 7 and 14 days; (B) 21 days and (C) 28 days relative to protein levels of naïve animals of comparative ages, measured by BDNF ELISA (n = 4 rats/group, fold change values represented as mean ± SEM, *p < 0.05, **p < 0.01, ***p < 0.001, One-way ANOVA with Tukey post-hoc test for multiple comparisons for (A), student's t-test for (B) and (C)).

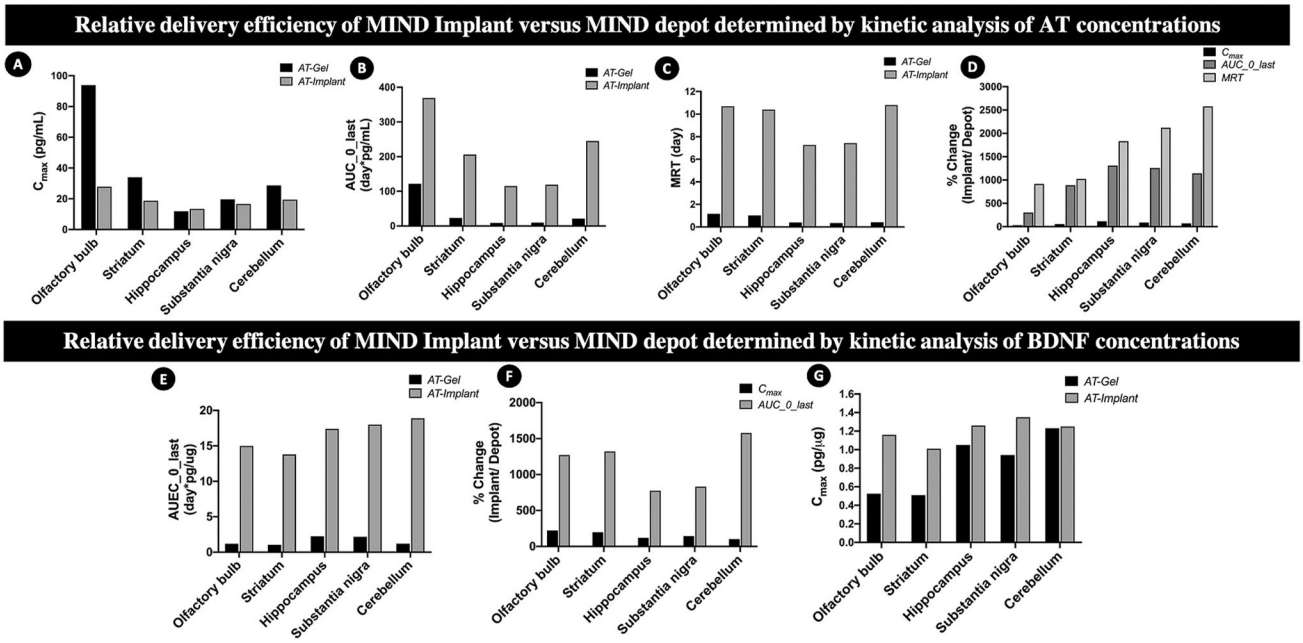

Fig. 5. Relative delivery efficiency of BDNF antagNAT (AT) using MIND implant as compared to the MIND AT-Gel depot reported previously by our group [28].

Top panels: Comparisons by kinetic analysis of AT concentrations by noncompartmental analysis with respect to (A) C_{max}; (B)AUC; (C) MRT; (D) overall percent changes. Bottom panels: Comparisons by kinetic analysis of BDNF protein concentrations by noncompartmental analysis with respect to (E) C_{max}; (F) AUEC; (G) overall percent changes.

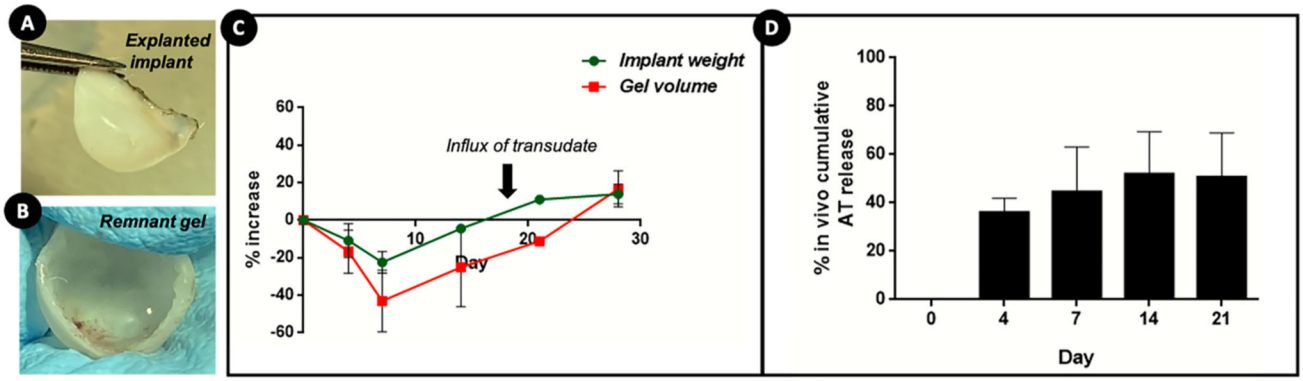

Fig. 6. Characterisation of the course of *in vivo* BDNF AntagoNAT (AT) release from osmotic core-shell implant.

(A) MIND implant explanted from the rat submucosal space after euthanasia; (B) explanted implant cut open to retrieve the remnant gel volume; (C) quantification of changes in the weights of explanted implants and remnant gel volumes with respect to time; (D) *in vivo* cumulative release of BDNF AT from core-shell implants determined using nanodrop spectrophotometer.

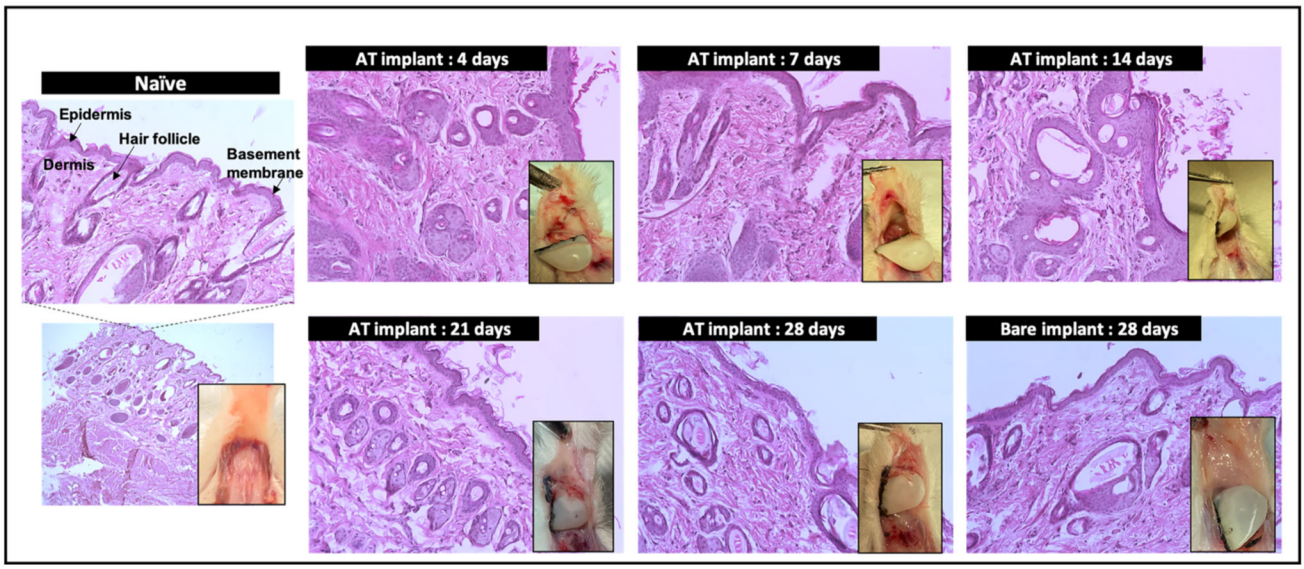

Fig. 7. Histological evaluation of nasal tissues retrieved from the MIND implantation site of rats after euthanasia at different timepoints.

Inset images show the photographs of tissue with the implants at different time points. H & E stained images (scale bar corresponds to 100 μm).

Table 1

Pharmacokinetic parameters of BDNF AT following BDNF AT implant administration via MIND technique.

Parameter	Unit	Olfactory bulb	Striatum	Hippocampus	Substantia nigra	Cerebellum
t_{max}	*Day*	4	4	7	7	7
C_{max}	$pg*mL^{-1}$	27.8	18.7	13.4	16.6	19.4
AUC^{a}	$pg*mL^{-1}*day$	369	206	115	119	245
$AUMC^{a}$	$pg*mL^{-1}*day$ [2]	3950	2140	834	885	2630
MRT^{a}	*Day*	10.7	10.4	7.27	7.43	10.8

[a]Estimated from time zero to last time point.

Table 2

Pharmacokinetic parameters of BDNF response following BDNF AT implant administration via MIND technique.

Parameter	Unit	Olfactory bulb	Striatum	Hippocampus	Substantia nigra	Cerebellum
t_{max}	*day*	14	14	14	14	7
C_{max}	$Pg*\mu g\ protein^{-1}$	1.16	1.01	1.26	1.35	1.25
$AUEC$ [a]	$pg*\mu g\ protein^{-1}*day$	15.0	13.8	17.4	18.0	18.9

[a]Estimated from time zero to last time point.